Analyzing Multiple Cotunneling Distance for Gold Nanoparticle Arrays at Cryogenic Temperatures

THESIS

submitted in partial fulfillment of the
requirements for the degree of

MASTER OF SCIENCE
in
PHYSICS

Author :	Isabelle Heukensfeldt Jansen
Student ID :	1577093
Supervisor :	Dr.ir. Sense Jan van der Molen
2^{nd} corrector :	Dr. Milan Allan

Leiden, The Netherlands, July 6, 2016

Analyzing Multiple Cotunneling Distance for Gold Nanoparticle Arrays at Cryogenic Temperatures

Isabelle Heukensfeldt Jansen

Huygens-Kamerlingh Onnes Laboratory, Leiden University
P.O. Box 9500, 2300 RA Leiden, The Netherlands

July 6, 2016

Abstract

In this work, we investigate methods to determine the average length for cotunneling in self-assembled gold nanoparticle arrays spaced with alkanethiols. Cotunneling currents can be as low as 10 fA, requiring the development of robust measurement techniques to lower the noise floor. We present a comparison of different methods for finding the effective cotunneling length N. Preliminary findings on a variety of arrays indicate the onset of the cotunneling regime, but that there is no distinction in N between choice of alkanethiol in the array.

Contents

Chapter 1

Introduction

The study of molecular electronics seeks to understand the charge transport properties of molecules and integrate them into nanodevices. The field takes conventional electronic components–switches [1], diodes [2], transistors [3]– and shrink them down to the molecular level. Arrays of nanoparticles have recently been studied as a means for probing charge transport through molecules [4]. An array provides reliability by measuring the spatial average over many parallel junctions [5], allowing stable measurements under ambient conditions of many molecules in parallel. The transport properties of the array depend on the molecular species used to space or bridge the nanoparticles, either during the formation of the array, or by exchanging one molecular species for another after the array is established. They thus function as a "molecular breadboard" [4].

Due to their small radius, these nanoparticles function as isolated charging islands with large charging energy. While their behavior is Ohmic at higher temperatures, current is suppressed due to Coulomb blockade [6] below a certain threshold temperature. In this regime, electron transport across the array happens through cotunneling [7, 8], which is the transfer of two or more electrons through intermediate virtual states. Arising from random quantum fluctuations in charge, a cotunneling current requiring N tunneling hops scales as the molecular conductance (related to the probability of one tunneling event) to the power N [5]. Since the molecular species in the array can be exchanged (or be a molecular switch with on/off states), this power-law dependence can enhance the difference in current between two states of the array.

In order to make use of this, we need to establish a reliable way of measuring N. This involves refining the data acquisition to accurately measure low currents, sometimes as low as 10 fA.

In this project, we focused on developing data analysis tools to explore cotunneling mechanics. Preliminary measurements used gold nanoparticle arrays that were self-assembled using heptane-, octane-, nonane-, or decanethiol as a spacer molecule between the particles. The current response to voltage at cryogenic temperatures of these arrays exhibited Coulomb blockade. These IV curves were used to compare two independent methods of calculating the number of cotunneling hops involved in charge transport. On some arrays, the molecular species of the array was exchanged with a bridging molecule, oligo(phenylene 3-ethynylene) (OPE3), a conjugated molecule that has approximately 50 times the conductance the resistance of alkanethiols, to provide comparison between an array with two states.

Chapter 2

Cotunneling

Cotunneling is a macroscopic quantum process [7] in which electrons may cross a classically-forbidden array of nanoparticles. In this chapter, we present the mechanism for cotunneling and the process' role in enhancing a nanoparticle array's molecular signature.

2.1 Coulomb Blockade

Isolated metal spheres have a capacitance proportional to their radius and the dielectric constant of the surrounding materials, $C = 4\pi\epsilon r$. Placing a charge q on these charging islands requires a charging energy of $E_c = q^2/2C$. As the radius of the sphere decreases, its charging energy increases. When the radius of the sphere is on the order of nanometers, the energy required to place one additional electron on the sphere is on the same scale as other energies relevant to charge transport, namely applied voltage and thermal energy.

Coulomb blockade occurs when the energy required to place an electron on a charging island is greater than either the electrostatic energy eV or the thermal energy k_BT of the contacts: $E_c > eV, k_BT$. Figure 2.1 shows the relevant energy levels. If in equilibrium, there are n electrons on the nanoparticle, then the $n+1$th electron going onto the particle must have E_c more energy to charge the sphere.

In the Coulomb blockade regime, current is suppressed because there are no electrons that have that energy [6]. Similarly, there are unoccupied states (holes) that the charging island's nth electron could tunnel into (Fig. 2.1a). When eV or k_BT is sufficiently large (Figs. 2.1b and 2.1c respectively), the blockade is overcome, and current flows sequentially. The

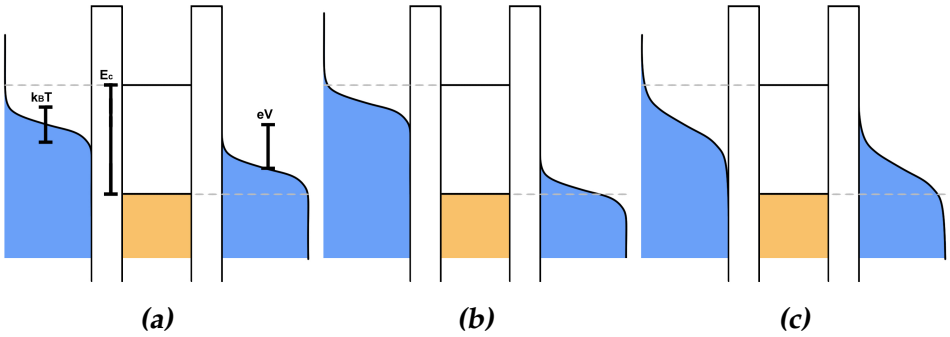

Figure 2.1: *(a) When $E_c > k_BT, eV$, no electrons have the required energy to tunnel onto or off of the charging island. (b) Coulomb blockade overcome by applied voltage. (c) Coulomb blockade overcome by thermal energy.*

ground state of the charging island can be raised or lowered relative to the contacts using a back gate, which changes the temperature and voltage needed to overcome Coulomb blockade.

2.2 Cotunneling

Interestingly, in the Coulomb blockade regime current can still flow through the junction through a cotunneling process [7]. Individually, both electrons and holes are classically forbidden from entering the charging island, as this violates conservation of energy. However, due to Heisenberg's Uncertainty Principle, virtual states may temporarily violate conservation of energy, provided that the lifetime of the state is short. This allows for quantum charge fluctuations, allowing electrons (or holes) from the metal contacts to exist in a virtual state on the charging island with a virtual state lifetime proportional to $1/E_c$. When both an electron from the electron source and a hole from the electron sink tunnel onto the charging island (Fig. 2.2a A and B, respectively) within this time window, the island is left in a energetically-allowed state, and an electron has effectively passed across the junction.

The cotunneling process happens through two tunneling events (Fig. 2.2a). The relation between the initial and final energy for each state (Fig. 2.2b) leads to two types of electron transport. In elastic transport, a single electron tunnels across both barriers. This type of transport only dominates in systems where the quantum energy level spacing is sufficiently large (i.e. quantum dot [10]). More frequently, electrons undergo inelastic transport, shown in Fig 2.2b, which leaves the charging island in an excited state [9].

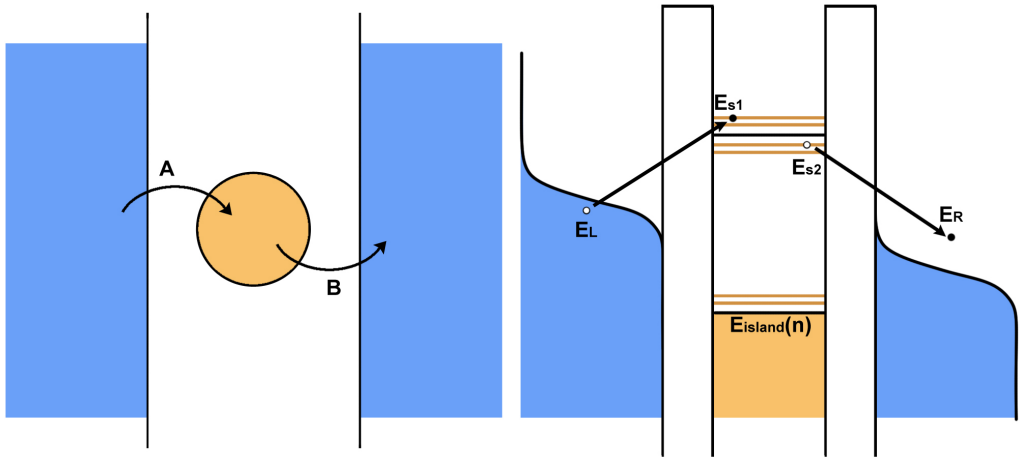

Figure 2.2: *(a) For current to flow during Coulomb blockade, electrons must enter and leave the charging island within the same time window. (b) The energy levels involved in the cotunneling process. E_L, E_R, E_{s1}, E_{s2} are quantum energy levels (relative to the grounded state of the system), while E_{island} is the electrostatic potential of the charging island. In inelastic cotunneling, the charging island is left in an excited state once the electron transport is complete, while in elastic cotunneling, $E_{s1} = E_{s2}$. Image modified from [9].*

Except in systems of quantum dots, inelastic cotunneling is more common, and dominates the overall current-voltage characteristics of the junction.

The inelastic cotunneling current across the junction was derived by Nazarov et al. [7] from the Fermi Golden Rule which determines the rate of transfer between two states:

$$\Gamma_{i,f} = \frac{2\pi}{\hbar} \left| \langle i| \hat{H} |f\rangle \right|^2 \delta \left(E_f - E_i \right). \tag{2.1}$$

As cotunneling happens through virtual states, it is appropriate to apply perturbation theory, and sum over all possible virtual states:

$$\langle i| \hat{H} |f\rangle = \sum_v \frac{\langle i| \hat{H} |v\rangle \langle v| \hat{H} |f\rangle}{E_i - E_v}. \tag{2.2}$$

$\langle i| \hat{H} |v\rangle$ and $\langle v| \hat{H} |f\rangle$ are the probability amplitudes for an electron tunneling event to happen, which are the transmission probability amplitudes t_L and t_R for the left and the right contacts respectively. With each contact biased such that the voltage drop across the whole junction is $V = V_L - V_R$, the initial energy of the system as a whole is

$$E_i = E_{\text{island}}(n) + E_L + eV_L + E_{s2}, \tag{2.3}$$

Either the electron entering or leaving the island can tunnel first; this gives rise to two distinct pathways. When the electron tunnels onto the island first, the island becomes negatively charged, and the virtual state energy becomes:

$$E_{v1} = E_{\text{island}}(n+1) + E_{s1} + E_{s2}. \tag{2.4}$$

Conversely, when the electron tunnels off the island first, the island is positively charged, and energy of the virtual state of the system is

$$E_{v2} = E_{\text{island}}(n-1) + E_L + eV_L + E_R + eV_R. \tag{2.5}$$

The energy of each tunneling hop can be rewritten as $\mathcal{E}_L = E_{s1} - E_L$ and $\mathcal{E}_R = E_R - E_{s2}$ for the electron and hole hop respectively. The charging energy of island relates to a difference in E_{island}: $E_c(n) = E_{\text{island}}(n+1) - E_{\text{island}}(n)$. Thus, the rate of a single electron across the junction becomes

$$\Gamma_{i,f} = \frac{2\pi}{\hbar}\left|\sum_{v1}\frac{|t_L|^2|t_R|^2}{-E_c(n)-\mathcal{E}_L+eV_L} + \sum_{v2}\frac{|t_R|^2|t_L|^2}{E_c(n-1)+\mathcal{E}_R-eV_R}\right|^2 \delta\left(E_f - E_i\right), \tag{2.6}$$

where the sum over states has been expanded to include both types of virtual states. The current through the junction is the sum over all initial and final states. Converting the sum to an integral over energy yields

$$\Gamma = \frac{2\pi}{\hbar}\mathcal{T}_L\mathcal{T}_R \iiiint_E \left|\frac{1}{\Delta E_L} + \frac{1}{\Delta E_R}\right|^2 \delta\left(\mathcal{E}_L + \mathcal{E}_R - eV\right) f_{FD}\, dE_L\, dE_R\, dE_{s1}\, dE_{s2}, \tag{2.7}$$
$$f_{FD} = f(E_L)[1-f(E_{s1})]f(E_{s2})[1-f(E_R)]$$

where $\mathcal{T}_{\mathcal{L}(\mathcal{R})} \equiv |t_{L(R)}|^2$ is the transmission probability across one of the island's barriers, related to the conductance across the barrier by $G_{\mathcal{T}} = G_0\mathcal{T}$ (the conductance quantum $G_0 = e^2/h$). The integral over virtual states can be taken outside of the squared term since electrons tunnel individually, and therefore there are no cross-terms. At a low temperature T and voltage bias V, solving this integral leads to the inelastic cotunneling current having the form:

$$I = \frac{G_0}{6\pi^2}\mathcal{T}_L\mathcal{T}_R\frac{\left[(eV)^2 + (2\pi k_B T)^2\right]}{E_C^2}V. \tag{2.8}$$

As expected for a current relying on two statistically-independent events, the current is proportional to the product of each event's probability $\mathcal{T}$. The lifetime of the virtual state is proportional to $1/E_c$; this gets squared in the conversion from probability amplitude to probability.

Version of July 6, 2016– Created July 6, 2016 - 13:39

2.3 Multiple Cotunneling

The cotunneling mechanism can be expanded to include arrays with more than one charging island between the metal contacts. Cotunneling in this case may involve more than two electron tunneling hops before the electron ends up in a classically-allowed state. A junction with $n-1$ islands between the contacts requires a total of n tunneling hops (cotunneling + sequential) to transport electrons across the junction.

In multiple cotunneling, electrons might reach a classically-allowed state before reaching the other contact. Between each charging island is a voltage drop $V_{jct} = V/n$, assuming the voltage drops linearly across the array (See Fig. 2.3). Depending on the energy level of the electron leaving

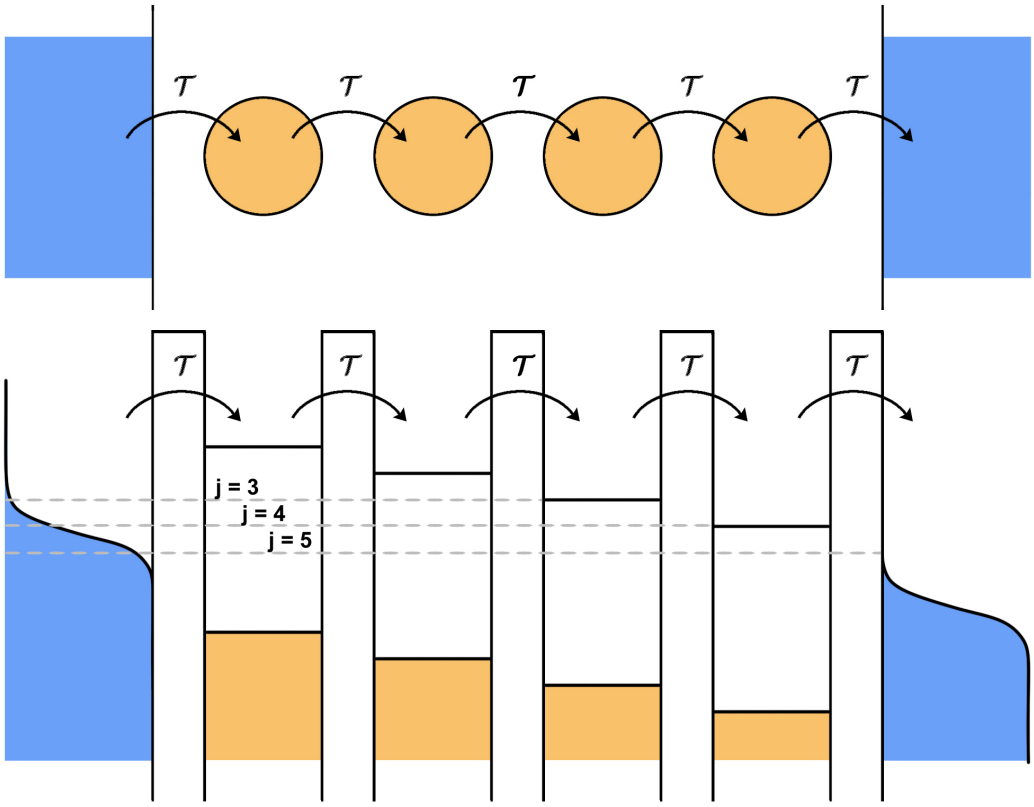

Figure 2.3: *When multiple charging islands span the distance between two contacts, electron transport occurs via a series of virtual states until they reach a classically allowed state. Depending on the initial energy level of the electron, the number of tunneling hops involved in the process varies. The energy levels required for 3, 4, and 5 hops is marked. For an array of 4 charging islands, a total of 5 tunneling hops (cotunneling + sequential) are required.*

Version of July 6, 2016– Created July 6, 2016 - 13:39

the contact, the electron might find a classically-allowed state on a nearby charging island $j-1$ before reaching the final contact. With j independent tunneling hops involved, the rate at which this happens is proportional to $\mathcal{T}^j$. Once classically on the charging island, the electron can transverse the remainder of the array with a rate proportional to the probability of tunneling only once. Since $\mathcal{T}^j \ll \mathcal{T}$, the rate-limiting step is the initial cotunneling process, and sequential tunneling afterwards does not affect the overall current. At finite temperatures, the spread of the electron Fermi distribution of the contacts (k_BT) suggests there are multiple allowed values for j. The total current through the array is therefore the sum over all the individual contributions of current for each value of j, and can be written as [11]

$$I \propto G_0 V_{jct} \sum_j \mathcal{T}^j \left(\frac{k_B^2 T^2 + e^2 V_{jct}^2}{E_C^2} \right)^{j-1} \exp\left(-\frac{\frac{E_c}{j} - jeV_{jct}}{k_B T} \right). \tag{2.9}$$

This has a similar form to Eq. 2.8.

2.3.1 C1, C2, C3 Regimes

In an array, multiple cotunneling happens along many paths. As a result, the current over the array has a dependency on the spatial average over all paths and lengths of cotunneling along those paths. We define N as a weighted average over j, and thus, the j which results in the largest current contribution. N can be found by treating j like a continuous variable and finding the maximum of Eq. 2.9 [5]:

$$\frac{\partial}{\partial j} \left(-\frac{E_c}{jk_BT} + j\frac{eV_{jct}}{k_BT} + j \ln \mathcal{T} + (j-1) \ln \frac{k_B^2 T^2 + e^2 V_{jct}^2}{E_C^2} \right) \Bigg|_{j \equiv N} = 0. \tag{2.10}$$

At zero voltage bias, the solution to this reduces down to

$$N = \sqrt{\frac{E_c}{k_B T \ln[e^2 R_\mathcal{T}/h]}} \tag{2.11}$$

Here, we use $\mathcal{T} = 1/G_0 R_\mathcal{T} = h/e^2 R_\mathcal{T}$, as $R_\mathcal{T}$ more directly relates to a measurable quantity, and so is useful for later discussion. Applying the voltage-dependent solution of N back into Eq. 2.9 gives an approximate cotunneling current:

$$I \propto \frac{E_c^2 V_{jct}}{e^2 V_{jct}^2 + k_B^2 T^2} \exp\left[-2\sqrt{\frac{E_c}{k_B T}} \sqrt{\ln \frac{G_0 R_\mathcal{T} E_c^2}{e^2 V_{jct}^2 + k_B^2 T^2}} - \frac{eV_{jct}}{k_B T} \right]. \tag{2.12}$$

The above equation can be reduced into a more manageable form by splitting the response into three regimes:

C1 Linear regime. $I = GV$ when $eV_{jct} \ll k_B T$

C2 Power-law regime. $I \propto V^{2N-1}$ when $k_B T < eV_{jct} < k_B T \ln\left[\frac{e^2}{h} R_{\mathcal{T}}\right]$

C3 Exponential regime. $I \propto E_C \exp\left[-\sqrt{\frac{V^*}{V}}\right]$ when $eV_{jct} > k_B T \ln\left[\frac{e^2}{h} R_{\mathcal{T}}\right]$

In the C1 regime, G takes the form

$$G \propto \left(\frac{h}{e^2 R_{\mathcal{T}}}\right)^N \left(\frac{k_B T}{E_C}\right)^{2N-2} \exp\left[-\frac{E_C}{N k_B T}\right]. \tag{2.13}$$

This represents intuitive cotunneling behavior, where each hop as a statistically independent event must occur within a certain time window. The total current is proportional to the product of the probabilities of each hop,

$$I \propto \prod_n^N \mathcal{T}_n = \mathcal{T}^N = \left(\frac{h}{e^2 R_{\mathcal{T}}}\right)^N, \tag{2.14}$$

in the same way that Eq. 2.8 is. Simplifying Eq. 2.13 by defining a characteristic temperature $k_B T^* = 4E_C \ln\left[e^2 R_{\mathcal{T}} E_C^2 / h k_B^2 T^2\right]$, it takes the form of the Efros-Shklovskii (ES) law [12] describing variable-range hopping:

$$G \propto \frac{E_C^2}{k_B^2 T^2} \exp\left[-\sqrt{\frac{T^*}{T}}\right]. \tag{2.15}$$

In the C2 regime, the average number of cotunneling hops is directly visible in the exponent. Since it does not rely on other physical quantities such as $R_{\mathcal{T}}$ or E_C, it provides a stable way of determining N of the network.

In the C3 regime, the electron transport follows an ES-like law, using an electric field dependence instead of a temperature dependence [13]. The characteristic voltage V^*, given by

$$V^* = \frac{E_C}{e}\left(\ln \frac{e^2 R_{\mathcal{T}}}{h}\right)^2, \tag{2.16}$$

has no dependence on N. Electron transport happens through a voltage-activated hopping mechanism, and there is no significant cotunneling in the C3 regime.

2.4 Molecular Bridges

To this point, we have discussed the mechanism through which cotunneling occurs, with little consideration for the role that the molecular species in the array plays. A nanoparticle has a large enough capacitance that an array of nanoparticles exhibits Coulomb blockade and cotunneling [5, 9, 11, 13]. A gold nanoparticle array can have various molecular species introduced into the array by exchanging the current molecules, changing the inter-particle resistance $R_{\mathcal{T}}$.

At low bias, the current is inversely proportional to $R_{\mathcal{T}}$. This dependence makes a cotunneling array able to enhance the difference between molecular species in the array. By measuring the same array with a change in $R_{\mathcal{T}}$, the ratio of the current across the array before and after exchanging the molecular species can be directly compared to find a value for N, assuming N remains constant. The relative currents between two states of the array then reduce to

$$\frac{I_1}{I_2} = \left(\frac{R_{\mathcal{T},2}}{R_{\mathcal{T},1}}\right)^N. \tag{2.17}$$

When N is large (N has been found to go as high as 4 or 5 [5]), the distinction between two different molecular bridges (or a molecular switch with an on/off state) becomes more pronounced.

In this work, we used two types of molecular species between the nanoparticles. As a high-resistance spacer molecule, we used alkanethiols of different lengths: heptane-, octane-, nonane-, and decane- thiol (C7, C8, C9, C10) (See Fig. 2.4a). In some arrays, we exchanged the alkanethiols for thiol-capped oligo(phenylene 3-ethynylene) (OPE3) to form a bridge between two nanoparticles (See Fig. 2.4b). Because OPE3 is a conjugated molecule, the shape of the orbitals allows it to have a conductance approximately 50 times higher than that of octanethiol. At room temperature, this is directly proportional to the conductance of the array.

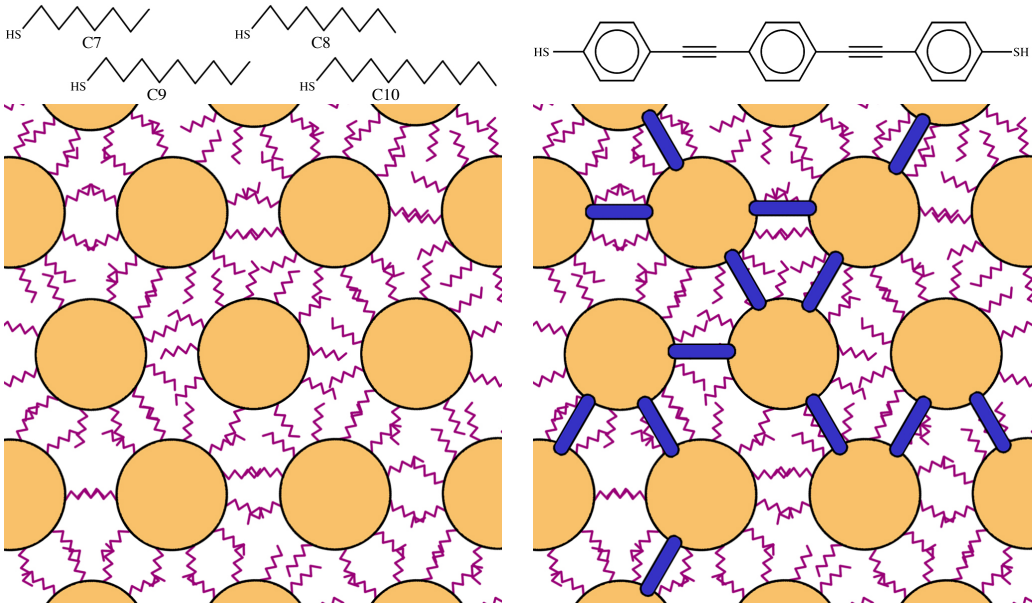

Figure 2.4: *Gold nanoparticle arrays (Image not to scale). The diameter of the nanoparticles is 10 nm, while the inter-particle spacing is around 2.5 nm. (a) Low-conductance alkanethiols act as a spacer for the nanoparticles. (b) During exchange, some alkanethiols are replaced with OPE3, a bridging molecule that connects two nanoparticles.*

Chapter 3

Data Acquisition and Methods

To observe cotunneling, it is necessary to have a device composed of a series of nanoparticles with a high charging energy between two metal contacts. In this chapter, we describe methods of preparation for such a device: a gold nanoparticle array. Cotunneling is seen through the current response at low temperatures, with currents as low as 10 fA. Measuring currents this low requires both refined data acquisition techniques and post-acquisition analysis methods.

3.1 Device Fabrication

Device fabrication was done [14] using the following process. The nanoparticles were synthesized using the Turkevich method [15], and separated via centrifuge to get particles with a diameter of 10 ± 1 nm. The nanoparticles are covered in alkanethiols, and dissolved into a chloroform solution.

To form the array, 60 to 70 μL of the solution is pipetted on the convex surface of a drop of water in a Teflon cup [16]. As the chloroform evaporates, the nanoparticles form a hexagonal close-packed (HCP) lattice on the surface. This lattice is stamped using polydimethylsiloxane (PDMS) onto lithographically-defined gold contacts, shown in Fig. 3.1. The total surface area L along the length of the contacts is 5 mm, and the contacts are separated by a width W of 500 nm, yielding an aspect ratio of 10,000.

The spacing of the network lattice is determined by the alkanethiol, which surround the nanoparticle in a shell. It has been experimentally determined that the inter-particle spacing for C8 is 2.6 $\pm$1.4 nm [17]; inter-particle distances for arrays with other alkanethiols scale proportional to the length of the alkanethiol. With a HCP lattice, this leaves approximately

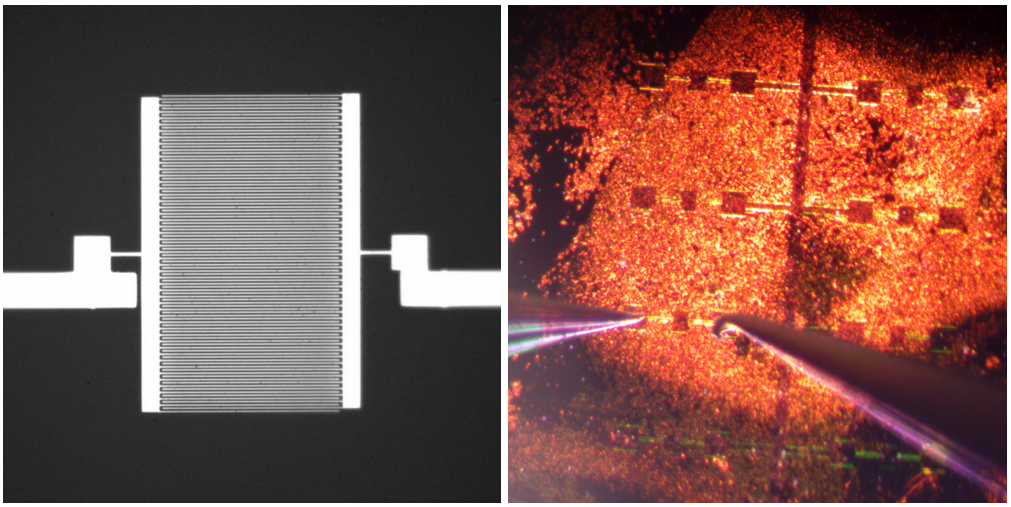

(a) ***(b)***

Figure 3.1: *(a) Gold contacts before the array is stamped onto them. The fingers of a comb mesh to create a long surface area between the two sides. (b) Devices with nanoparticle array stamped on.*

42±6 nanoparticles between the contacts.

To exchange the molecular bridge of the sample from alkanethiols to OPE3, the sample was placed in a solution of OPE3 in tetrahydrofuran (THF) prepared inside a N_2 atmosphere (glovebox) [18]. Because the solution has a high concentration of OPE3, some of the alkanethiols in the shell surrounding the nanoparticle will randomly exchange with the OPE3 in the solution. This process was shown to have completed in approximately 30 minutes [19], but to be certain, samples were left in solution for a minimum of an hour. If needed, reversing this process (back-exchange) simply requires using alkanethiols in the solution instead of OPE3.

3.2 Data Acquisition

The IV characteristic of the cotunneling devices were measured using a NI USB-6341 DAQ system and a Femto DLPCA-200 Low Noise Current Amplifier. The DAQ system functioned both as a voltage source and as a tool for recording the amplified current. Before starting the measurement, the DAQ system was configured to sweep across voltages in a range in a full triangle wave, providing both trace and retrace measurements of the current.

For measured devices, the average resistance could vary from 1 kΩ

(OPE3, room-temperature) to 1 TΩ (C10, low temperature and bias). To compensate for the variation of the current across orders of magnitude, two measurement parameters are automatically determined at the start of each voltage sweep: the current amplification and the measurement frequency. The current amplifier is capable of amplifying incoming current from 10^3 to 10^9 V/A. To increase measurement accuracy, the current amplifier was set to the highest order of magnitude that could be used without overloading (saturating) the current amplifier. At maximum current amplification, the accuracy could be further increased by increasing the time over which the current is measured (decreasing the measurement frequency). The DAQ was set to measure at a rate of 250,000 samples/second. At 1000 Hz, the recorded current for each voltage point is the average over 250 measurements. As the frequency of the measurement decreased, more values were used to calculate the current, though the time taken to run the measurement program proportionally increased.

At each temperature, most devices had two IV curves measured: once with a "high" voltage amplitude of 1 V and once with a "low" voltage amplitude of 50 mV. This allowed the current amplifier to switch amplification factor in between curves and improve the accuracy of the low-bias measurements.

3.2.1 Cryostat Control

For cotunneling to occur, the array first needs to be in the Coulomb blockade regime. This happens at low temperatures, under 100 K. To measure IV curves over temperatures ranging from 300 K down to 1.6 K, samples were loaded into an Oxford Instruments Teslatron CF cryostat. We developed a driver for the cryostat written in Python to automate the measurement process, complete with a simple Graphical User Interface (See Fig. 3.2) and backend hooks to allow for inclusion into other measurement programs.

In addition to providing a human-readable wrapper to the native programming language of the cryostat (e.g. "SET: DEV: MB1.T1: TEMP: LOOP: TSET: 2.5K" becomes "set_temperature_setpoint(2.5)"), the code provides several aggregate functions for finer control. One additional functionality is automatic determination of the temperature stability for the variable-temperature insert chamber (VTI chamber) and the sample holder insert. Given a certain tolerance (read from a configuration file, but recommended between 0.2% and 5%), the temperature is deemed to be stable based on the following four criteria:

1. The temperature has been measured for at least a minute.

2. The mean of the temperature over the last minute is near the temperature setpoint: |mean - setpoint|<setpoint $\times$ tolerance.

3. The temperature is not drifting: the slope of the temperature over the last minute is near zero.

4. The temperature is not fluctuating: standard deviation $<$ setpoint $\times$ tolerance.

At very low temperatures, the effective tolerance needed to be increased, as even reasonable fluctuations in the temperature would cause the stability conditions to fail. This was achieved by setting the lower boundary for the value of the setpoint times the tolerance to 0.01, generally effective for under 5 K.

In addition to providing more monitoring tools, the module also increases the rate of cooling down the cryostat. The VTI chamber, sample insert, and chamber pressure operate on independent control feedback loops. This can slow the rate of cooling in two ways. The VTI chamber

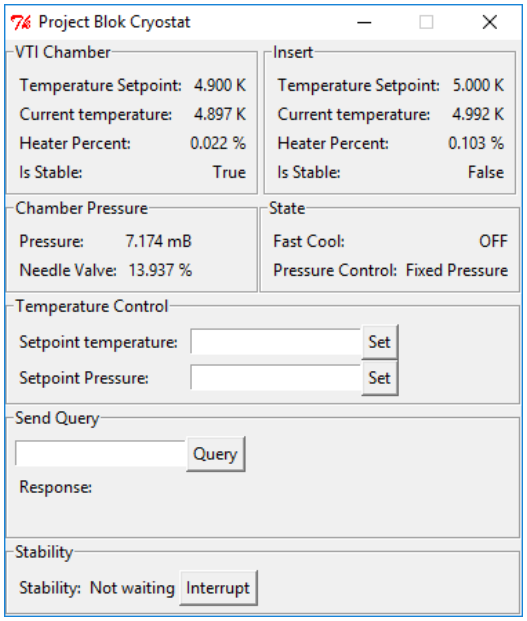

Figure 3.2: *Graphical User Interface to control the Oxford Instruments Teslatron CF cryostat. The interface includes optional "Temperature Control" and "Send Query" boxes that may be turned off to provide a monitor during programmed measurements*

gets its cooling power from a cooling plate, with the pressure inside the chamber determining its ability to thermalize. When the pressure is too low, the chamber cannot dump its heat into it and will have larger fluctuations in temperature; too high, and the gas heats up the chamber (a concern at under 10 K). As part of the aggregate "set_temperature" function, the module adjusts the pressure of the chamber to match the temperature conditions.

The sample insert gets its cooling power from the VTI chamber, which therefore must maintain a temperature difference for the insert to be able to dump heat. However, as the VTI cools directly from the cooling plate, it often reaches its temperature setpoint and stabilizes more quickly. This results in an increasingly small temperature difference between the insert and the VTI chamber, and the insert has trouble thermalizing over the last few degrees. To speed up the stabilization time, some basic communication between the two temperature controls was established. When the temperature setpoint was set to more than 30 K lower than the previous temperature, the module would turn off the heater for the VTI chamber completely, allowing the temperature to "free fall" until the insert was at the temperature setpoint. The VTI chamber heater was then turned back on, allowing both the insert and the VTI chamber to stabilize at the same time. This, the pressure control, and the stability calculations were written to be non-blocking, allowing measurement programs to run "intuitively" and have further commands execute while the cryostat cools.

Appendix A shows example measurement code to loop through a list of temperatures, set the cryostat to each temperature, and run a LabView program once the temperature stabilizes. This code allowed us to cut down the measurement time from fully measuring 2 devices over the course of 3 days, to measuring 6 devices over the course of a single day. Each device was measured at the following temperatures (listed in Kelvin):

Cool down				Warm up	
300	75	17.5	5	5	100
250	50	15	4	10	150
200	40	12.5	3	15	200
150	30	10	2	20	250
100	20	7.5	1.6	50	300

Table 3.1

The devices were first cooled from 300 K to 1.6 K, and then measured

again as the cryostat warmed up, to ensure there was no time dependence in the IV curves.

3.3 Data Corrections

Many of the IV curves were digitally modified after the measurement to correct errors introduced by the measuring equipment. The current amplifier uses an instrumentation amplifier, which can introduce several artifacts into the measurement.

Figure 3.3 shows a typical IV measurement on both the trace (green) and retrace (blue) of the voltage. Hysteresis in the measurement is introduced through the current amplifier due to a tendency to overshoot the true current value at the beginning of the measurement. The amount of overshoot depends on the measuring rate and the amplification order; thus, for a single curve, the current overshoot on the voltage increase and decrease is the same amount. The average of the measured current (black) therefore cancels out the positive overshoot when the voltage is increasing with the negative overshoot when the voltage is decreasing. Additionally, averaging out the voltage trace and retrace dramatically decreases the interference in the measurement, seen in the Fourier transform in Fig. 3.4. The frequency spectrum loses its spiky, even-odd frequency alternation that is the result of taking the Fast Fourier Transform over a triangular function, but also all but the largest peaks. Since each pair of two points that get averaged together have a different time offset between them (largest at $V = 0$, smallest at $|V| = V_{max}$), interference gets smoothed away in the averaging, at the cost of slightly increasing white noise instead.

No current flows through the junction at zero bias, and the IV curve should reflect that. However, the instrumentation amplifier adds an offset to the measurement due to leakage current, which is non-negligible when the resistance is high. To account for the noise in the original measurement, the offset is taken from a linear fit of the curve in the C1 regime ($eV_{jct} \ll k_B T$). To confirm this properly accounts for the offset, calculated values in Chapter 4 treat both the IV curve and its reflection around the origin ($I(V)$ and $-I(-V)$) equally.

Figure 3.5 shows the IV curves of a single device with both hysteresis and offset corrections applied. The non-linear behavior characteristic of Coulomb blockade emerges at temperatures under 100 K. This shows up both in the 1 V amplitude sweep (left), and, to a lesser degree, in the zoomed-in 50 mV amplitude sweep which is mainly situated in the lin-

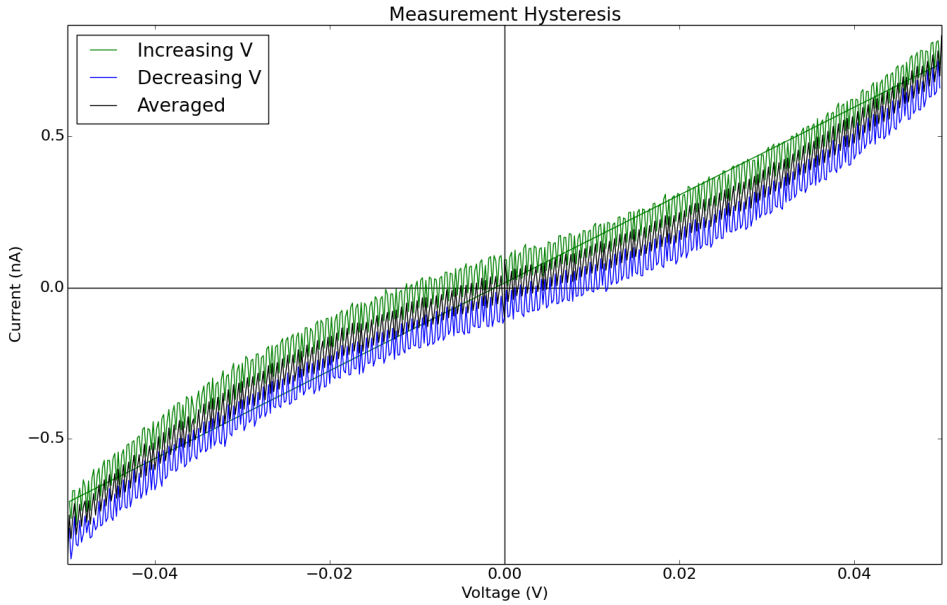

Figure 3.3: *Typical IV curve measured on a C7 network at 10 K. Hysteresis in the loop between trace (green) and retrace(blue) of the device comes from the capacitors attached to the instrumentation amplifier. The average of the two curves (black) corrects for the overshoot of the value.*

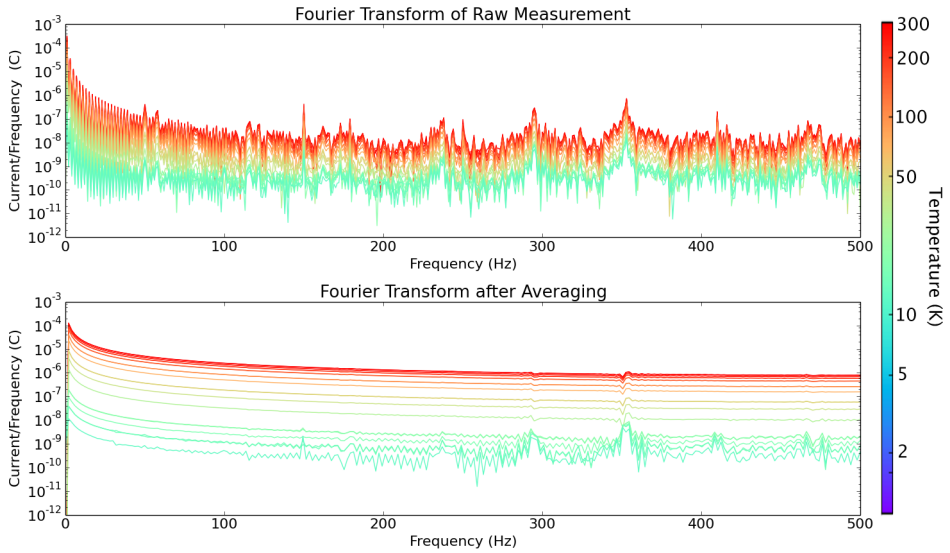

Figure 3.4: *FFT of IV curves for C7 device across a range of temperatures. (Top) Original measurements. (Bottom) Taking the average of the voltage trace and retrace decreases the interference due to outside electronics. Temperatures shown here range from 12.5 K to 300 K (see Table 3.1 for full list). Lower temperatures were measured at a different frequency.*

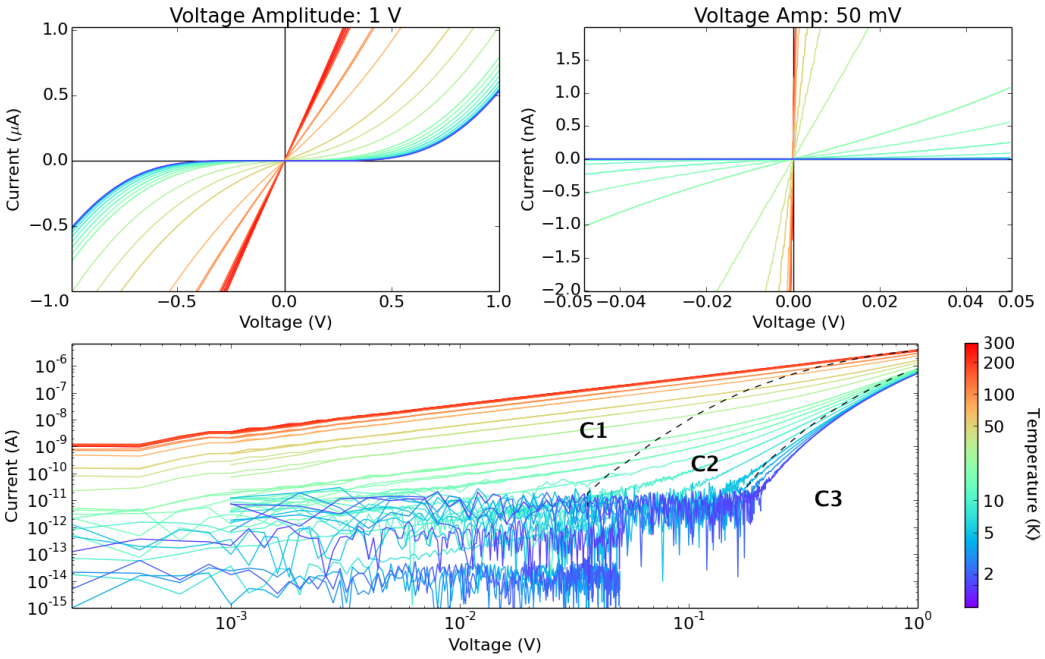

Figure 3.5: *Corrected IV curves over a range of temperatures from 1.6 K to 300 K for a C7 network exchanged with OPE3. (top left) IV measurements with a voltage amplitude of 1 V and (top right) 50 mV. (bottom) Log-log plot showing both sets of curves. Dashed lines represent the boundaries between the C1, C2, and C3 regimes. The noise floor varies depending on the current amplification factor and averaging time. See Table 3.1 for full list of temperatures.*

ear C1 regime. Both sweeps are also shown on the same plot (bottom) on a log-log scale. In this view, it is simple to see when the noise floor of a measurement at a given amplification is reached: the current flattens out to a constant, noisy value. This is especially prominent at the lowest temperatures.

The dashed black lines show the boundaries between the C1, C2, and C3 regimes. Following the derivation of the regimes by Dayen et al. [5], the separation of the regimes was determined by finding the appropriate voltage for a given temperature, and matching the voltage with the current value to trace a temperature-dependent line. The boundary between the C1 and C2 regime occurs at

$$V_{1-2} = \frac{N_{NP} k_B T}{e}, \tag{3.1}$$

where N_{NP} is the average number of nanoparticles connecting the two contacts, approximated to 40 as described above. Between the C2 and C3 regimes, the boundary is given by

$$V_{2-3} = \frac{N_{NP} k_B T}{e} \ln\left[\frac{e^2}{h} R_{\mathcal{T}}\right]. \tag{3.2}$$

For a square-shaped HCP network of connected resistors, the overall resistance across the network R is proportional to the resistance of the individual connections $R_{\mathcal{T}}$ by an approximate factor of 0.7 ($R \approx 0.7 R_{\mathcal{T}}$) [20]. This holds when the network is not in Coulomb blockade at high temperatures. To determine the boundaries of the C2-C3 regime, $R_{\mathcal{T}}$ is approximated from the resistance of the junction at 300 K and the aspect ratio L/W of the device, as the device functions as many square-shaped networks in parallel:

$$R_{\mathcal{T}} \approx \frac{L/W}{0.7} R_{300K} = \frac{10,000}{0.7} R_{300K}. \tag{3.3}$$

As V_{2-3} contains the log of $R_{\mathcal{T}}$, this approximation holds up against introduced errors.

3.4 Zero-bias Conductance

For many reasons, such as finding $R_{\mathcal{T}}$ or determining N (as will be described next chapter), it is useful to have the zero-bias differential conductance of an IV curve (or its inverse, the zero-bias differential resistance). When dealing with numerical data, the slope is determined by a linear fit.

Due to the non-linear nature of the IV curves, the fit cannot be applied to the whole voltage range at once. However, too small a range means the resulting slope will be affected by noise. Thus, it is appropriate to determine the optimal window Δv for a fit ranging over $V_{\text{bias}} \pm \Delta v$.

Figure 3.6 shows fitted zero-bias resistance of a set of curves as a function of the voltage window. Resistance (1/fitted slope) was chosen in order to highlight changes. As expected, the value at high temperatures remains constant no matter the window. As the temperature decreases, the noise at the beginning of each plot increases. On the other end, the resistance sharply decreases as the window outgrows the linear region. The peak in resistance indicates non-linear behavior in the curve. To fit for conductance over a linear region, we used the smallest window that avoided noise, in this case 0.15 V.

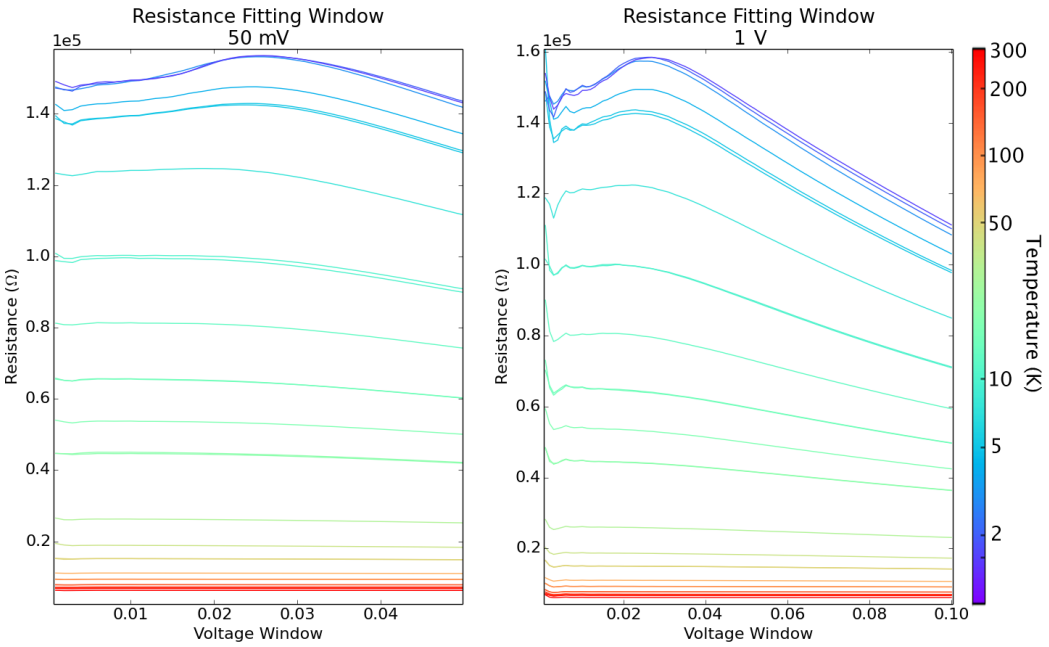

Figure 3.6: *Average resistance at zero-bias as a function of the width of the fitting window, for both the fine and coarse voltage measurements. See Table 3.1 for full list of temperatures.*

Chapter 4

Cotunneling Length

To confirm the robustness of the data analysis methods, the IV curves of several arrays spaced by alkanethiols of different lengths were measured at different temperatures. Here we discuss different methods for extracting the optimal cotunneling length N, and compare N's temperature evolution across different arrays.

4.1 Comparison of C1 and C2 Regime

Within the two regimes dependent on the cotunneling process (C1 and C2), there are two ways to determine the optimal number of cotunneling hops independent of each other. In the C1 linear regime, the conductance G of the junction is inversely proportional to $(R_{\mathcal{T}})^N$. Without knowing the precise factor, it is still possible to find N by comparing the ratio of conductances with and without OPE3 molecular bridges by using Eq. 2.17. Working under the assumption that at high temperatures, the junction is fully out of the cotunneling regime and therefore N is 1, the logarithm of the ratio of the current can be normalized to find N without needing any additional information:

$$N(V,T) = \frac{\ln\left[I_1(V)/I_2(V)|_T\right]}{\ln\left[I_1(V)/I_2(V)|_{300K}\right]}. \tag{4.1}$$

At zero bias, current in this equation is replaced by the conductance of the curve, possible since the current response in the C1 regime is linear. Finding N using this method relies on the assumption that the same device will have the same average number of cotunneling hops when $R_{\mathcal{T}}$ changes, as

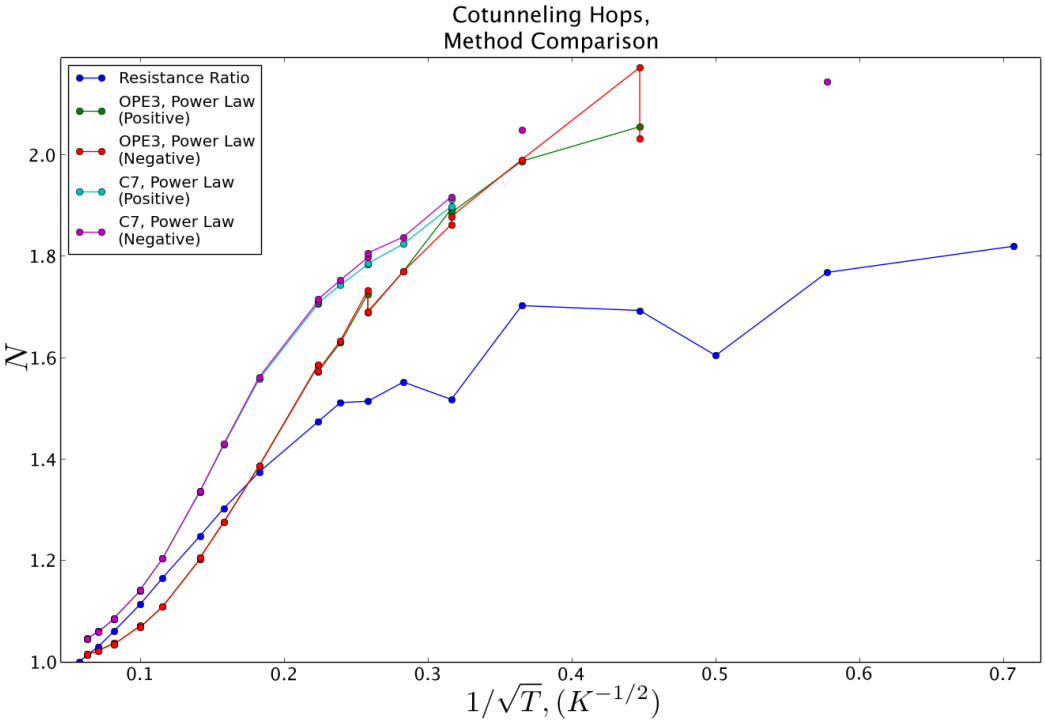

Figure 4.1: *N as a function of $1/\sqrt{T}$. For the same set of IV curves, N takes on different values depending on the method used to extract it. Since the C2 regime deals with higher currents, the power-law method used to extract N is more robust. N here is raw values extracted from a fitting routine, before accounting for sources of error.*

found by Dayen et al. [5]. This is largely a result of Eq. 2.11, which is only weakly dependent on $R_{\mathcal{T}}$.

In the C2 regime, the IV curve follows a power-law, $I = V^{\alpha}$, where $\alpha = 2N - 1$. The number of cotunneling hops in the network can be determined by a straight-forward power-law fit of the line. The end result is loosely dependent on N_{NP} and $R_{\mathcal{T}}$, which determine the boundaries between the C1, C2, and C3 regimes, and heavily dependent on having the correct offset correction of the curve. When N is calculated separately from both the voltage trace and retrace ($I(V)$ and $-I(-V)$), an incorrect offset gives a large difference in values; closely matching values thus serves as an indication that the offset is properly adjusted.

Figure 4.1 shows the results of both methods applied to the same set of IV curves from a single device. According to Eq. 2.11, N should be linear in $1/\sqrt{(T)}$. The power-law method for a network with C7 versus the same network with OPE3 finds a similar N value for all temperatures.

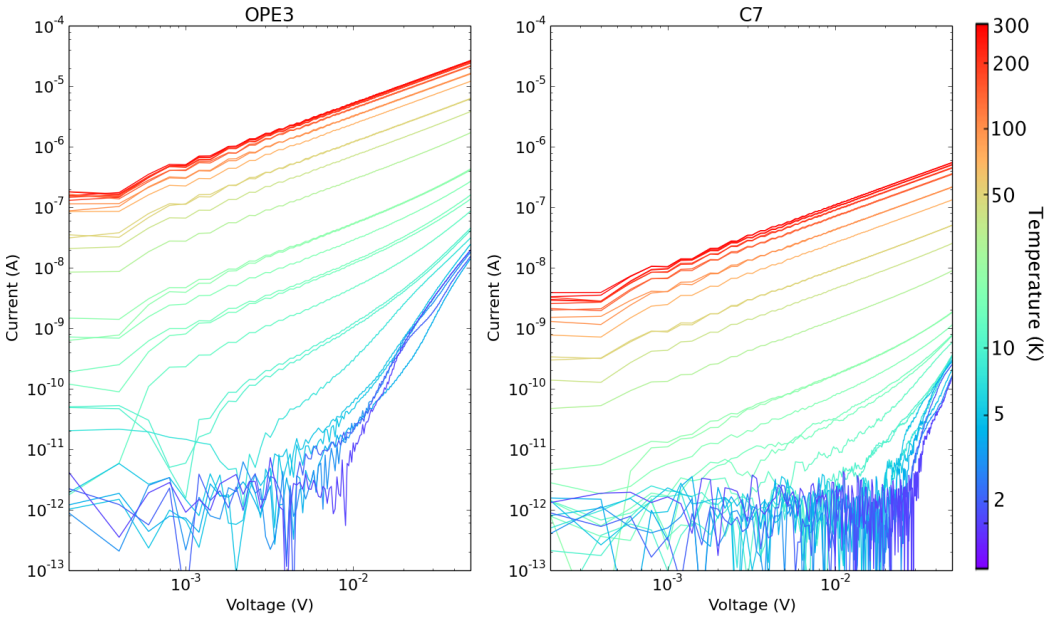

Figure 4.2: *Low voltage IV measurements (C1 regime) in a log-log plot for the same device shown in Fig. 4.1 with OPE3 and C7 in the array. The noise floor for both is 10 fA, but the C7 curves have a lower initial current, and therefore measures the noise floor for longer at lower temperatures.*

This validates the assumption that N is approximately the same for the calculation using the resistance ratio method.

At temperatures lower than 30 K, the two methods diverge dramatically. The N calculated via the resistance ratio method never enters the cotunneling regime ($N \geq 2$). This divergence likely arose because the resistance ratio method used low-voltage measurements. Such measurements, which dealt with smaller currents, were prone to noise. Even when the low-resistance OPE3 network had high currents, the resistance ratio method failed because the current in the high-resistance alkanethiol networks was not distinguishable from noise (See Fig. 4.2). Thus, N appears to continue to increase because I_{OPE3} changes to reflect the increasing N, while I_{C7} remains constant due to the noise floor. The resistance ratio method is therefore unreliable at low temperatures.

Because the power-law method applied to the C2 regime, it dealt with larger currents (See Fig. 4.3). χ^2 values for the power-law fit remained small above 10 K. Under this temperature, χ^2 values drastically increased as the noise floor overtook the C2 regime. Typically, the error in a fitted parameter comes from the covariance matrix; however, because a small

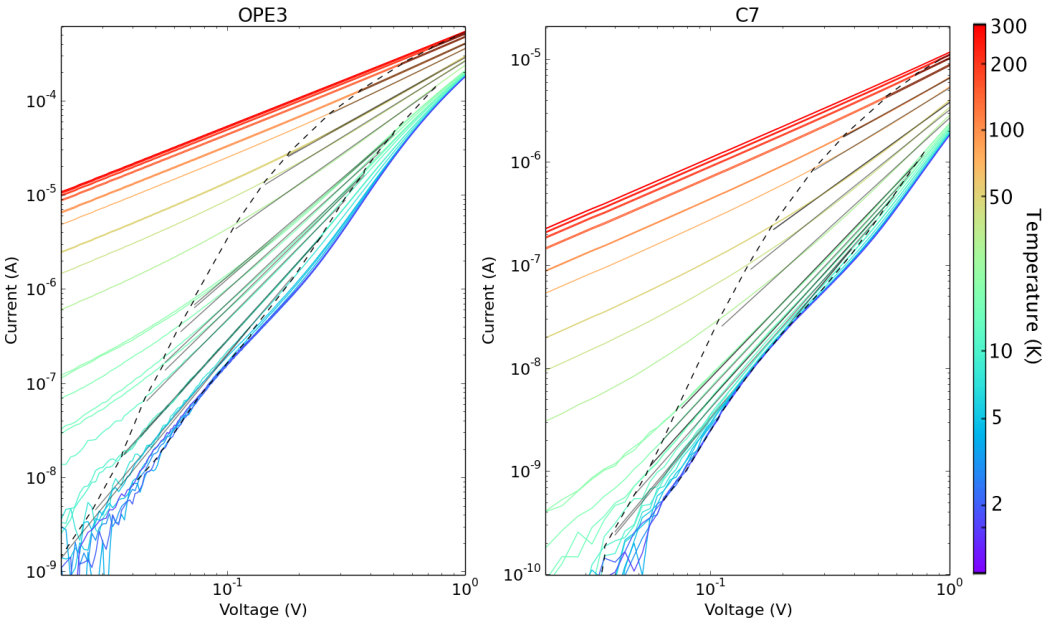

Figure 4.3: *Log-log plot of IV curves with a power-law fit of the C2 regime. As this type of fit is tolerant to noise in the measurement, the main source of error is non-exponential behavior in the regime; a difficult quantity to map to N-space.*

change in an exponent results in a large change in the fitted curve, a power-law fit is also more tolerant of noise in data and the covariance matrix was not a reasonable measure of confidence. χ^2 measures the goodness of a fit, but does not map into the error of N.

Since the power-law method only required an array to be measured with one type of connecting molecule, it allows for a more direct comparison of different types of arrays than the resistance-ratio method. The values for N discussed in the rest of chapter are calculated using the power-law method.

4.2 Inter-Network Comparison

We will now explore the relationship between N and the choice of heptane-, octane-, nonane-, or decanethiol (C7, C8, C9, C10) as the spacer molecule during self-assembly. As the capacitance of a nanoparticle depends not only on the radius, but also on the inter-particle distance, the average number of cotunneling hops N may be therefore tuneable through choice of alkanethiol. The effect of this tuning can be observed in the slope of the

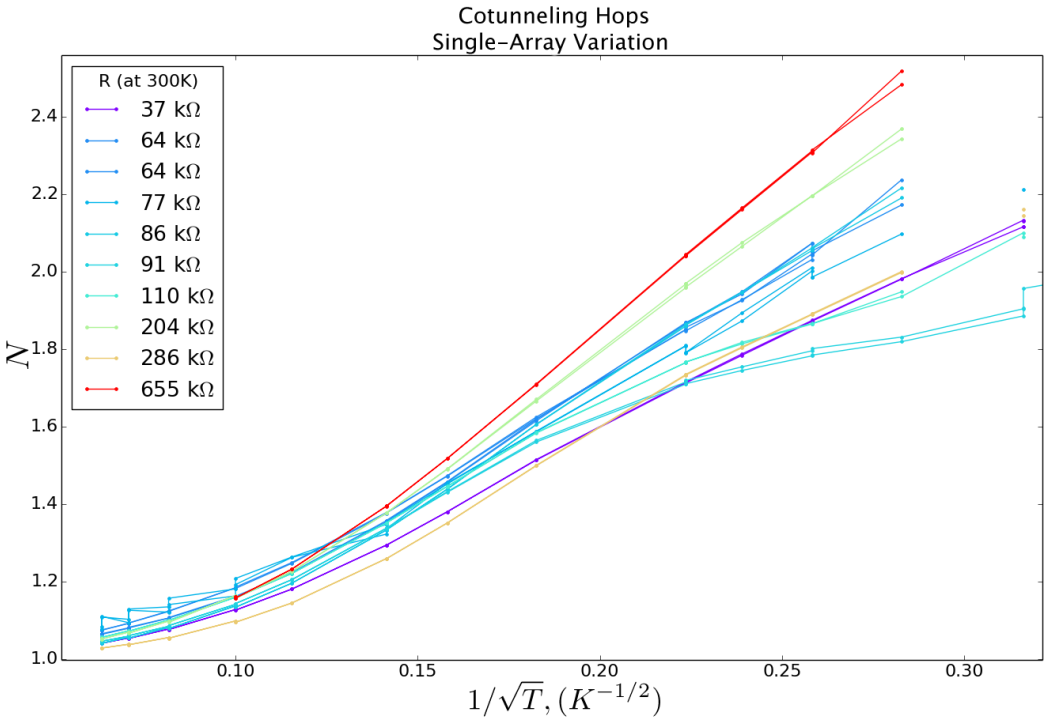

Figure 4.4: *Number of cotunneling hops N as a function of* $1/\sqrt{T}$ *at various locations on a C7-spaced array. Color of the line corresponds to the room-temperature resistance. At various temperatures, N shows no strong correlation to the resistance of the nanoparticle array at 300 K.*

plot of the N as a function of $1/\sqrt{T}$.

To have any meaningful comparison between different nanoparticle arrays, an array must be internally consistent. Figure 4.4 shows N measured at multiple locations across a C7 array. Each location had a different resistance at 300 K, ranging from 37 kΩ to 655 kΩ, indicating the quality of the nanoparticle array had local variations. Nonetheless, the behavior of N at different points in the array remained consistent, and was independent of the high-temperature resistance. This implies that we can use the mean of several curves to represent the behavior of the network.

Although an array might be consistent across internal variations, it remains to be seen if arrays with the same alkanethiol have the same N. Figure 4.5 compares two C7 arrays prepared using different heptanethiol/chloroform solutions. One array was less than a day old (blue), while the other was 15 days old (green). Although temperature trace and retrace measurements confirm no significant changes in an array over the

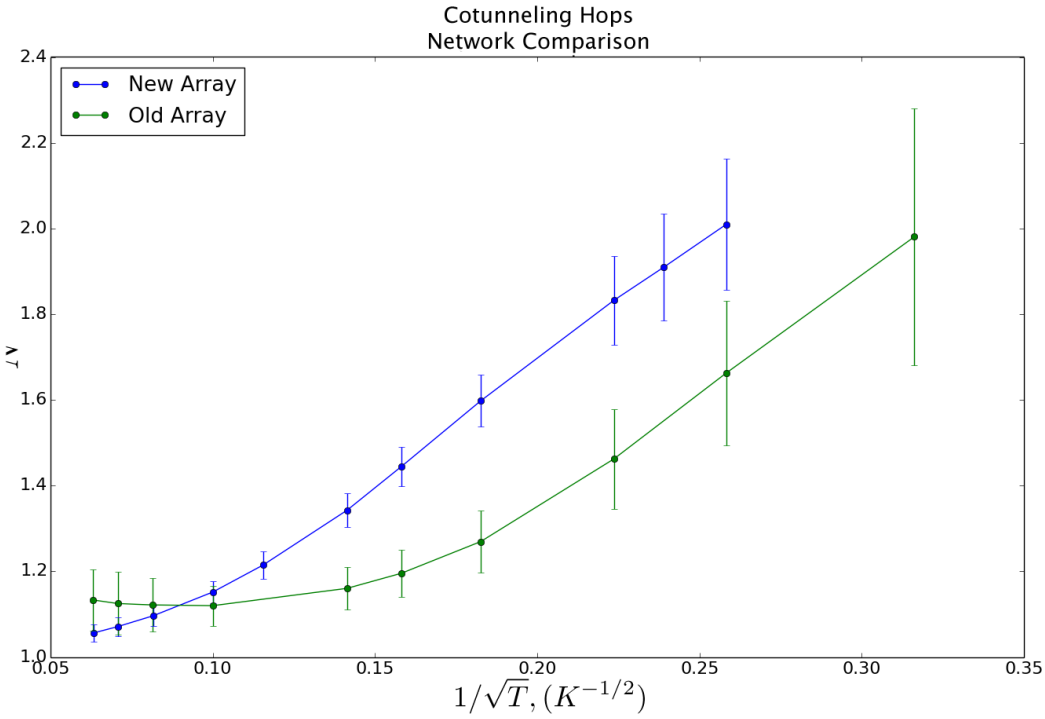

Figure 4.5: *N as a function of $1/\sqrt{T}$ for two separate arrays prepared with the same spacer molecule (C7) show a different temperature dependence. Since a single array has the same N at different locations (Fig. 4.4), the difference may be in the age of the array (blue-one day, green-two weeks), the change in preparation solution, or may be an inherent difference between similar arrays based on other preparation factors.*

timescale of the measurement, this might not be the case on a larger timescale. Compared to the relative consistency in Fig. 4.4 across the same array, N exhibits a different characteristic on the different arrays, even with the same spacer molecule: the older array distinctly shows an increase in non-linear $1/\sqrt{T}$ behavior. Whether this is a result of the nanoparticle solution, the age of the array, or a property of individual arrays cannot be determined at this time.

Given the difference in behavior between two similar arrays, the behavior across different length of alkanethiols, shown in Fig. 4.6, remains surprisingly consistent. The differences appear more as a result of statistical variation than as a result of a dependence on length. The arrays barely reaches the cotunneling regime ($N \geq 2$) at low temperatures; the C8 array (green) does not even reach cotunneling values yet at 7.5 K (the last point

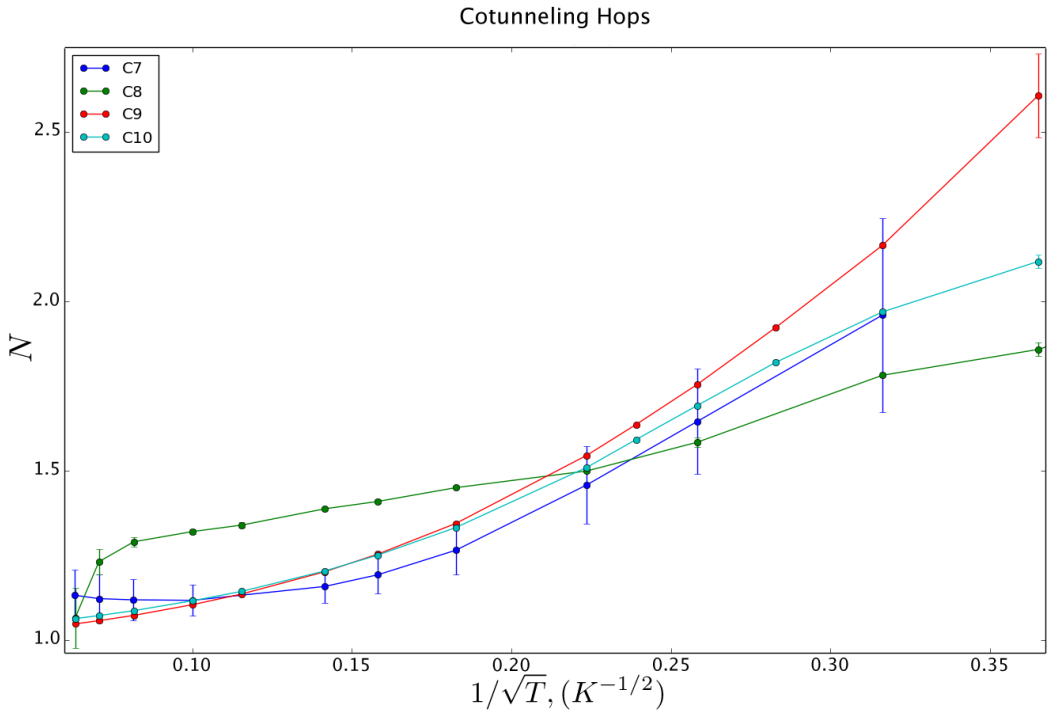

Figure 4.6: *N measured across several alkanethiols plotted as a function of $1/\sqrt{T}$ shows similar behavior in all lengths. When no standard deviation is shown, only a single device on the array was measured.*

of the plot). Since $N > 1$, there are some electrons cotunneling through the array, but the main transport still comes from sequential transport. This may be due to variations in the quality of the array, combined with the surface area of the contacts. Local defects may cause parts of the array to ”short circuit” and avoid Coulomb blockade. The larger the surface area of the two contacts, the higher the chance that a device contains such a defect. Because it would act as a path of least resistance, it would draw a majority of the current to dampen the effects of cotunneling. Creating devices with a shorter surface area may increase cotunneling behavior.

Chapter 5

Conclusion and Outlook

In HCP nanoparticle arrays spaced with by alkanethiols of various lengths, Coulomb blockade was observed to start under 100 K. The current response to voltage became increasingly non-linear as the temperature decreased. At these temperatures, the current could become as low as 10 fA, and required refined techniques to measure. We developed post-acquisition data analysis methods to correct artificial hysteresis and current offset introduced by the current amplification.

We compared two independent methods to determine N from a series of IV curves of an array. The first uses the ratio of low-bias conductance of the array connected with two different molecules to determine the temperature dependence of N. We have shown this method to be unreliable given the current measurement parameters, as it is limited by the noise floor of the current amplification. Determining N by an exponential fit of the C2 regime proved to be a more robust method since the higher voltage deals with larger currents. We applied this method to several preliminary samples to show that a single array was consistent across variations in the quality of the array, though there was some variation between different arrays both assembled with heptanethiol. The variation, possibly arising from a difference in array preparation, accounted for the variation seen in N across arrays prepared with different alkanethiols. This showed that thus far, there was no dependency for N on the length of the alkanethiol.

This lack of dependency may be as a result of the long surface area of the two metal contacts. All measurement only just reached the cotunneling regime of $N \geq 2$. With a longer surface area between contacts, the measured area of the array will include more defects that may act to "short circuit" parts of the network. We recommend determining if N relies on the surface area between the contacts. Decreasing the surface area would

also decrease the measured current. As some calculations in this work are already limited by the noise floor of the current amplification, future measurements should further improve data acquisition techniques.

Appendix A

Example Code for Cryostat Control

```
"""For a more in-depth example, see code package"""
import guiCryostat
import cCryostat
import threading
import win32com.client
import Tkinter

#list of temperatures to loop through
T = [300,250,200,150,100,50,10,5,4,3,2,1.6]

def make_gui(cryostat):
    root = Tkinter.Tk(None)
    gui = guiCryostat.guiCryostat(root, cryostat, control=False)
    gui.grid(row=0,column=0) #Add to main GUI window

    #Additional frames may be added to the window here,
     e.g. "Pause/Resume" program

    #run quit_app to close threads when done
    root.protocol("WM_DELETE_WINDOW", gui.quit_app)

    #Due to threading, main program runs concurrently with GUI
    #GUI can talk with main program through global variables
    thread = threading.Thread(target=root.mainloop)
    thread.daemon = True
    thread.start()

    return gui


#(More code next page)
```

```
#Initialization of main code
with cCryostat() as cryostat:
    paused = False
    LabVIEW = win32com.client.Dispatch("Labview.Application")

    make_gui(cryostat)


    #Labview Measurement Setup
    labview_path = 'D:\Labview programs\measurement.vi'
    VI = LabVIEW.getvireference(labview_path)
    VI._FlagAsMethod("Call")
    #Labview now can be run via python

    ###########Begin Main Loop###########
    for temperature in T:
        #set_temperature returns false if fails
        if cryostat.set_temperature(temperature):
            print "Setting temperature to %f K"%temperature
            cryostat.wait_for_stable()
            print "Temperature stable"

            VI.setcontrolvalue('Measurement param','0.01')
            #Sets parameters, which must be strings
            VI.Call()  # Run the VI

        else: print "Problem with setting to %f K"%temperature

    print "Closing Cryostat"
    gui.quit_app()
```

Bibliography

[1] Sense Jan van der Molen and Peter Liljeroth. Charge transport through molecular switches. *Journal of Physics: Condensed Matter*, 22(13):133001, 2010.

[2] Arieh Aviram and Mark A Ratner. Molecular rectifiers. *Chemical Physics Letters*, 29(2):277–283, 1974.

[3] Sergey Kubatkin, Andrey Danilov, Mattias Hjort, Jerome Cornil, Jean-Luc Bredas, Nicolai Stuhr-Hansen, Per Hedegård, and Thomas Bjørnholm. Single-electron transistor of a single organic molecule with access to several redox states. *Nature*, 425(6959):698–701, 2003.

[4] Jianhui Liao, Sander Blok, Sense Jan van der Molen, Sandra Diefenbach, Alexander W Holleitner, Christian Schönenberger, Anton Vladyka, and Michel Calame. Ordered nanoparticle arrays interconnected by molecular linkers: electronic and optoelectronic properties. *Chemical Society Reviews*, 44(4):999–1014, 2015.

[5] Jean-Francois Dayen, Edwin Devid, Mutta Venkata Kamalakar, Dmitry Golubev, Constant Guédon, Vina Faramarzi, Bernard Doudin, and Sense Jan van der Molen. Enhancing the molecular signature in molecule-nanoparticle networks via inelastic cotunneling. *Advanced Materials*, 25(3):400–404, 2013.

[6] LJ Geerligs, DV Averin, and JE Mooij. Observation of macroscopic quantum tunneling through the coulomb energy barrier. *Physical review letters*, 65(24):3037, 1990.

[7] DV Averin and Yu V Nazarov. Virtual electron diffusion during quantum tunneling of the electric charge. *Physical review letters*, 65(19):2446, 1990.

[8] TB Tran, IS Beloborodov, XM Lin, TP Bigioni, VM Vinokur, and HM Jaeger. Multiple cotunneling in large quantum dot arrays. *Physical review letters*, 95(7):076806, 2005.

[9] AE Hanna, MT Tuominen, and M Tinkham. Observation of elastic macroscopic quantum tunneling of the charge variable. *Physical review letters*, 68(21):3228, 1992.

[10] S De Franceschi, S Sasaki, JM Elzerman, WG Van Der Wiel, S Tarucha, and Leo P Kouwenhoven. Electron cotunneling in a semiconductor quantum dot. *Physical Review Letters*, 86(5):878, 2001.

[11] TB Tran, IS Beloborodov, Jingshi Hu, XM Lin, TF Rosenbaum, and HM Jaeger. Sequential tunneling and inelastic cotunneling in nanoparticle arrays. *Physical Review B*, 78(7):075437, 2008.

[12] A L Efros and B I Shklovskii. Coulomb gap and low temperature conductivity of disordered systems. *Journal of Physics C: Solid State Physics*, 8(4):L49, 1975.

[13] H Moreira, Q Yu, B Nadal, B Bresson, M Rosticher, N Lequeux, A Zimmers, and H Aubin. Electron cotunneling transport in gold nanocrystal arrays. *Physical review letters*, 107(17):176803, 2011.

[14] R. Overdevest. Characterizing Exchange in Nanoparticle Arrays (Unpublished). B.S. Thesis, Leiden University, the Netherlands, 2016.

[15] John Turkevich, Peter Cooper Stevenson, and James Hillier. A study of the nucleation and growth processes in the synthesis of colloidal gold. *Discussions of the Faraday Society*, 11:55–75, 1951.

[16] Venugopal Santhanam, Jia Liu, Rajan Agarwal, and Ronald P Andres. Self-assembly of uniform monolayer arrays of nanoparticles. *Langmuir*, 19(19):7881–7887, 2003.

[17] Laetitia Bernard. *Expanding the horizon of molecular electronics via nanoparticle assemblies*. PhD thesis, University of Basel, 2006.

[18] J. Liao, L. Bernard, M. Langer, C. Schönenberger, and M. Calame. Reversible formation of molecular junctions in 2d nanoparticle arrays. *Advanced Materials*, 18(18):2444–2447, 2006.

[19] P. Dieleman. Molecular exchange in 2D networks. B.S. Thesis, Leiden University, the Netherlands, 2011.

[20] David Atkinson and FJ Van Steenwijk. Infinite resistive lattices. *American Journal of Physics*, 67(6):486–492, 1999.